The importance of taking into account behavior irreversibilities when simulating the forming of textile composite reinforcements

T. Abdul Ghafour, J. Colmars, P. Boisse

Version of Record: https://www.sciencedirect.com/science/article/pii/S1359835X19303902
Manuscript_ba4df32fafdad395a90817cb47a3cdd9

The importance of taking into account behavior irreversibilities when simulating the forming of textile composite reinforcements

T. Abdul Ghafour[a], J. Colmars[a], P. Boisse[a*]

[a]Université de Lyon, LaMCoS, CNRS, INSA-Lyon, F-69621, France

Abstract

Simulations of the forming of textile composite reinforcements are generally based on elastic behavior models. However, the slippage between the fibers and the associated friction that occurs during shaping creates irreversibilities. The present paper describes the modeling and identification of these irreversibilities in a simple way from bending and bias extension tests. They were then integrated into forming simulations. The results of the simulations, that either took into account or neglected the irreversibilities, were compared in classic forming cases. It appeared that the geometries of the textile reinforcements after forming generally did not show any significant differences when irreversibilities where considered as opposed to when they were neglected. On the other hand, the internal forces in the reinforcement were found to differ depending on whether irreversibilities were taken into account. In addition, the results of elastic and inelastic simulations were very different in the case of a punch removal.

Keywords: A. Fabrics/textiles, C. Process Simulation, C. Finite element analysis (FEA), E. Forming, Irreversibilities.

1 Introduction

Continuous fiber reinforced composites are increasingly used in various fields of engineering due to their excellent weight-specific mechanical properties, which are advantageous in many areas of mobility and structural applications. The forming of these materials is often complex and simulations are necessary to avoid a time-consuming and costly development by trial and error. Several approaches and software have been developed over the last decades for the simulation of composite forming processes.

Such simulation makes it possible to determine the orientation of the fibers after forming but also the appearance and development of flaws such as wrinkles [1-6]. Simulations based on

* Corresponding author: philippe.boisse@insa-lyon.fr

pin joints (or fishnet algorithms) [7-9] are fast but do not take into account the mechanical behavior of the textile reinforcement nor the load boundary conditions. In order to consider these latter aspects, most approaches rely on the finite element method, which makes it possible to solve continuous media problems by taking into account the specific behavior of textile composite reinforcements and boundary conditions. These methods consider the forming process as a quasi-static problem and employ an implicit resolution scheme [10,11] or an explicit dynamic approach [1,2,12-15].

The main specificity of these forming simulations lies in the mechanical behavior of the textile reinforcements which are made up of continuous fibers. During deformation, relative slippage can occur between the fibers that are very stiff in tension and almost inextensible. This leads to a specific mechanical behavior where the stiffness of the reinforcement in the direction of the fibers is high while the other stiffnesses (shear, bending, transverse compression) are small.

The present article is focused on dry textile composite reinforcements. Their forming (sometimes called preforming) is carried out before the resin was injected into the LCM (liquid composites moulding) processes [16,17]. Simulations of this forming step are important since they determine the direction of the fibers, possible defects but also the volume fraction and architecture of the fiber yarns that define permeability [18-22]. These simulations are generally based on elastic [4,23,24-29], hypoelastic [30-32] and hyperelastic [33,34] behavior models. Viscoelastic models have been developed for the forming of prepreg, in particular thermoplastics [1,35-39]. In contrast, when modelling the forming of other materials, one most often uses irreversible behavior models. In particular sheet metal forming is modeled by elasto-plastic behavior laws [40-42].

During forming, the mechanical behavior of textile reinforcements has both reversible and irreversible components. The tensile elongations of the fibers are small and reversible and the bending deformations of the fibers are generally also reversible. However, slippages between the fibers, which give rise to in-plane and transverse shear strains on a macroscopic scale, are associated with friction and are irreversible. The question at hand is whether it is necessary to take these irreversibilities into account in textile composite reinforcements forming simulations or whether they can be neglected? The objective of this paper has thus been to, in a simple way, model the irreversibilities of the behavior of woven reinforcements and to take them into account during forming simulations. For this, there were two objectives. First

of all, to understand how irreversibilities modify the simulation results and, above all, to compare the simulation results when irreversibilities are taken into account as opposed to when they are not.

Inelastic models have been identified by bending tests and bias extension tests for two different textile composite reinforcements. Classical shapes with single and double curves have been analyzed: U-shape, hemisphere, tetrahedron and square-box shapes. It was found that, in most cases, the geometry of the textile reinforcements after forming was not significantly modified when behavior irreversibilities where taken into account as opposed to when they were neglected. On the other hand, the internal forces in the reinforcement could be modified by considering irreversibilities.

In the case of removal of the punch after forming, the simulations lead to a very different result depending on whether the elastic or anelastic models are taken into account. This shows that the behavior of a textile reinforcement during forming is inherently irreversible and that it must be described by an inelastic model in the general case. In the liquid infusion process, elastic simulations can be considered because the punch is not removed and the mold remains closed. This article generally considers forming processes without tool removal. The tool removal phase is nevertheless analyzed when forming a U-shape or a tetrahedron shape.

2 Inelastic behavior of textile composite reinforcements

2.1 Material and mechanical tests

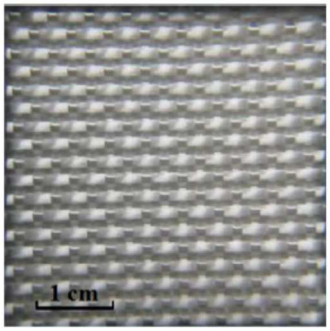

T1 : 3D orthogonal non-crimp woven glass fabric. (Thickness ≈ 3mm)

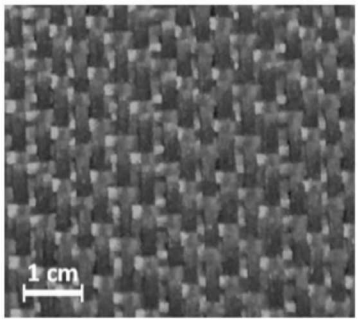

T2: carbon interlock Hexcel G1151 (Thickness ≈ 3mm)

Fig. 1. The analyzed textile composite reinforcements

This section highlights the inelastic behavior of two textile composite reinforcements: a 3-mm woven glass reinforcement (3D orthogonal non-crimp woven fabric [43,44]) and a 1-mm

carbon interlock (Hexcel G1151 [45,46]). In the following, the textile composite reinforcements shown in Fig. 1 are denoted T1 and T2. The objective of the tests was to highlight the irreversibility of the mechanical behavior. The bending behavior of textile reinforcements is specific. The slippage between the fibers leads to a much lower bending stiffness than that of the membrane [47-49]. The textile reinforcements T1 and T2 of this study were subjected to a three-point bending with loading/unloading (Fig. 2a). This test was used to test different interlock reinforcements [50,51]. The size of the specimens was 210 mm × 55 mm.

The in-plane shear behavior of textile reinforcements has been the subject of numerous studies [52-56], probably due to the fact that in-plane shear is the deformation mode that makes it possible to form surfaces with double curvatures. The in-plane shear behavior was characterized by Bias-Extension-Tests (Fig. 2b) and the size of the samples was 150 mm × 60 mm.

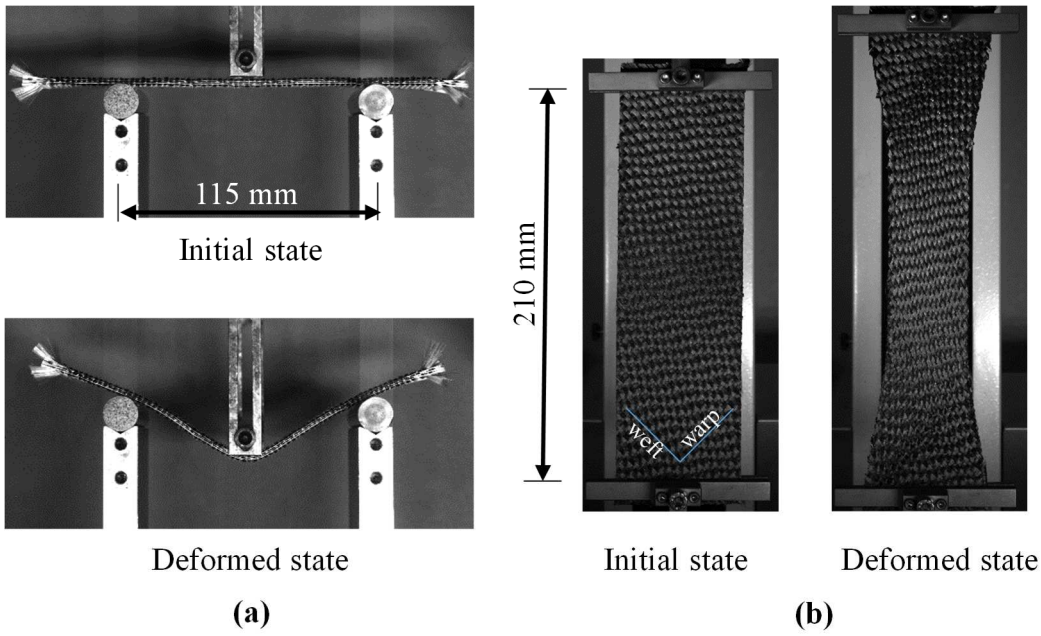

Fig. 2. (a) Three-point bending test on the fabric T1 (b) Bias-extension-test on the fabric T2

2.2 Irreversibility of the mechanical behavior

Fig. 3a shows the measured experimental load as a function of the central displacement for loading/unloading during bending of the textile reinforcements T1 (left) and T2 (right). Three point bending tests were performed with cylindrical loading pin and supports (with a 16 mm diameter). A Lloyd LF Plus 1 kN traction machine was used with a 100 N capacity sensor. All

experimental curves shown below were obtained after a minimum of three repetitions. The size of the specimens was selected as 210 mm × 55 mm in order to get a significant number of woven patterns.

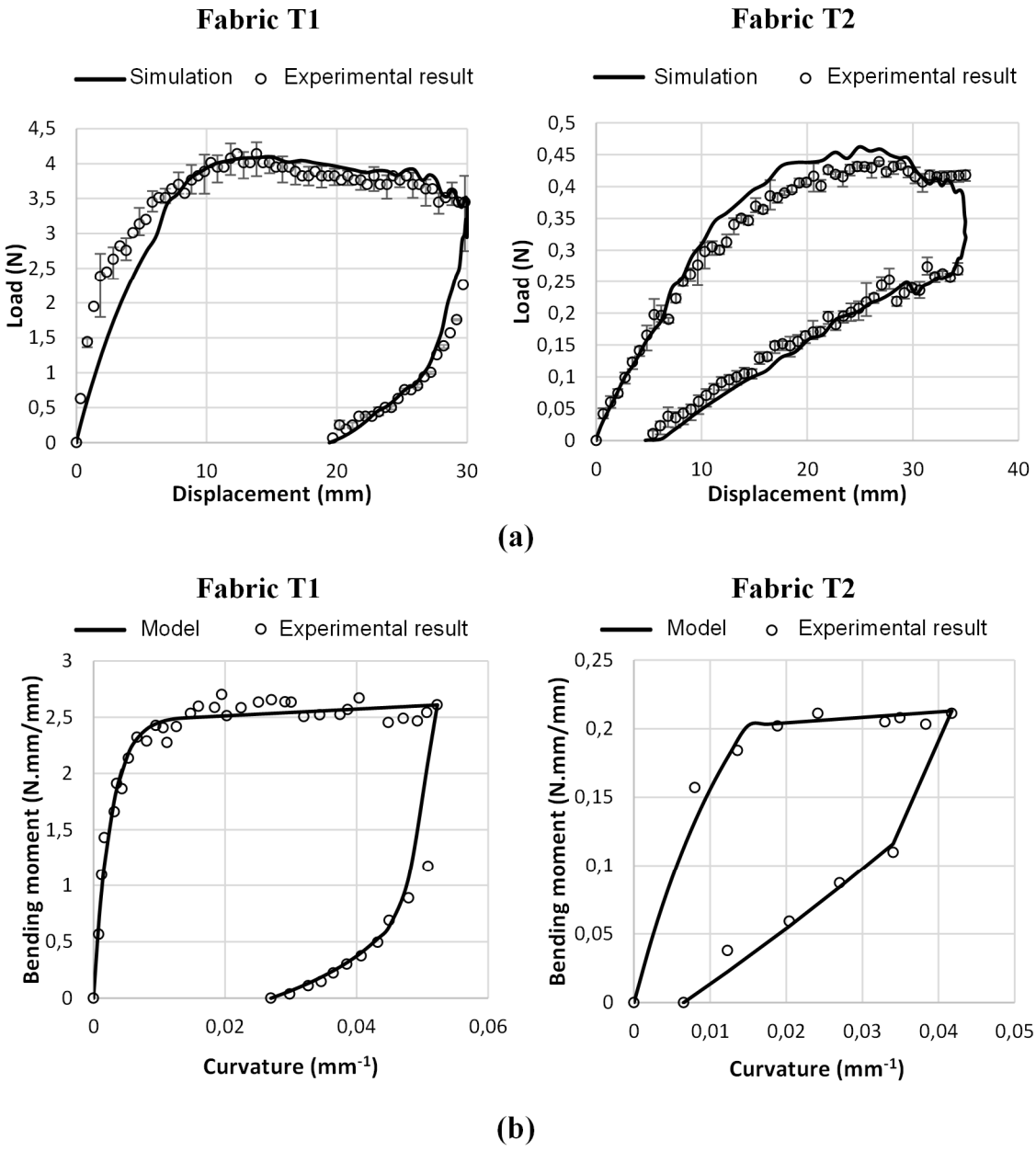

Fig. 3. Three point bending test: response to a loading/unloading. (a) Load versus displacement (average of three specimens: the standard deviation was approximately 0.25 N) (b) Bending moment versus curvature calculated from load-displacement curves.

The deformed configuration is obtained by optical measurement of the mean line at each time. After a polynomial approximation of the mean line, the curvature χ of the bending specimen was calculated by:

$$\chi(x) = \frac{f''(x)}{(1 + f'^2(x))^{\frac{3}{2}}} \quad (1)$$

Where $f'(x)$ and $f''(x)$ are, respectively, the first and second derivative of the polynomial function $f(x)$ with respect to x.

The bending moment was deducted from the load on the machine and the deformed configuration of the specimen (Fig. 3b), as in [57]. The finite element simulations presented below for draping simulations directly use this bending moment-curvature relation $M_b(\chi)$ for virtual work done by bending.

These figures clearly show that there were residual displacements and curvatures when the bending load was decreased to zero. The bending behavior of the two tested textile reinforcements was irreversible. Fig. 4 demonstrates that these irreversibilities increased in the case of loading/unloading cycle with a rising displacement and therefore curvature.

As in bending, the experimental in-plane shear curves for loading and unloading presented irreversibilities (Fig. 5a). During unloading, the load on the machine of the bias extension test decreased rapidly and became zero for a non-zero shear.

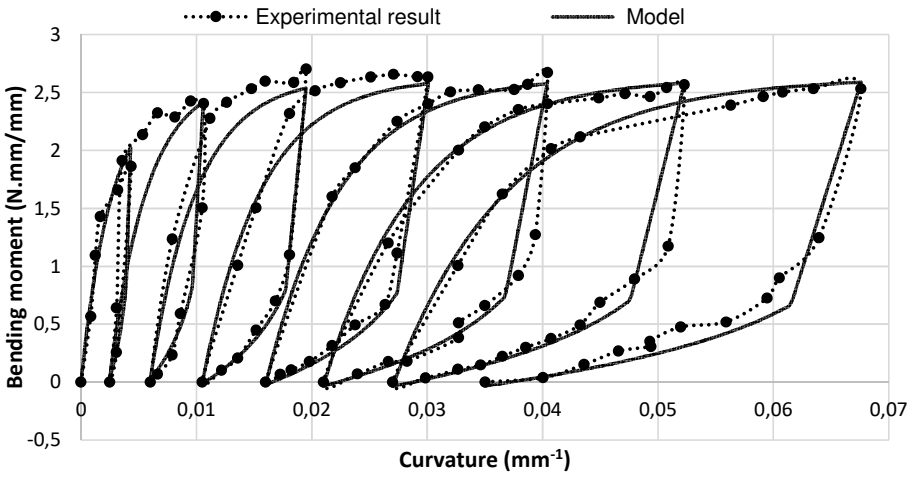

Fig. 4. Loading/unloadings during bending with increasing displacement.

Based on the assumption of inextensibility of the fibers and non-slip between the warp and weft yarns, the shear angle can be deduced from the displacement of the machine [46,52,54]. Similarly, the shear torque (or moment) on a unit woven cell can be expressed as a function of the load on the grip and geometric quantities [46,49,54]. The shear torque as a function of the shear angle $C_s(\gamma)$ is shown in Fig. 5b. The finite element simulations presented in the

sequel for draping simulations directly use this shear torque-shear angle relation for the virtual work by in-plane shear.

Fig. 5 clearly portrays that, for the two textile reinforcements studied here, the in-plane shear behavior was irreversible. When the shear force returned to zero, residual shear angles existed.

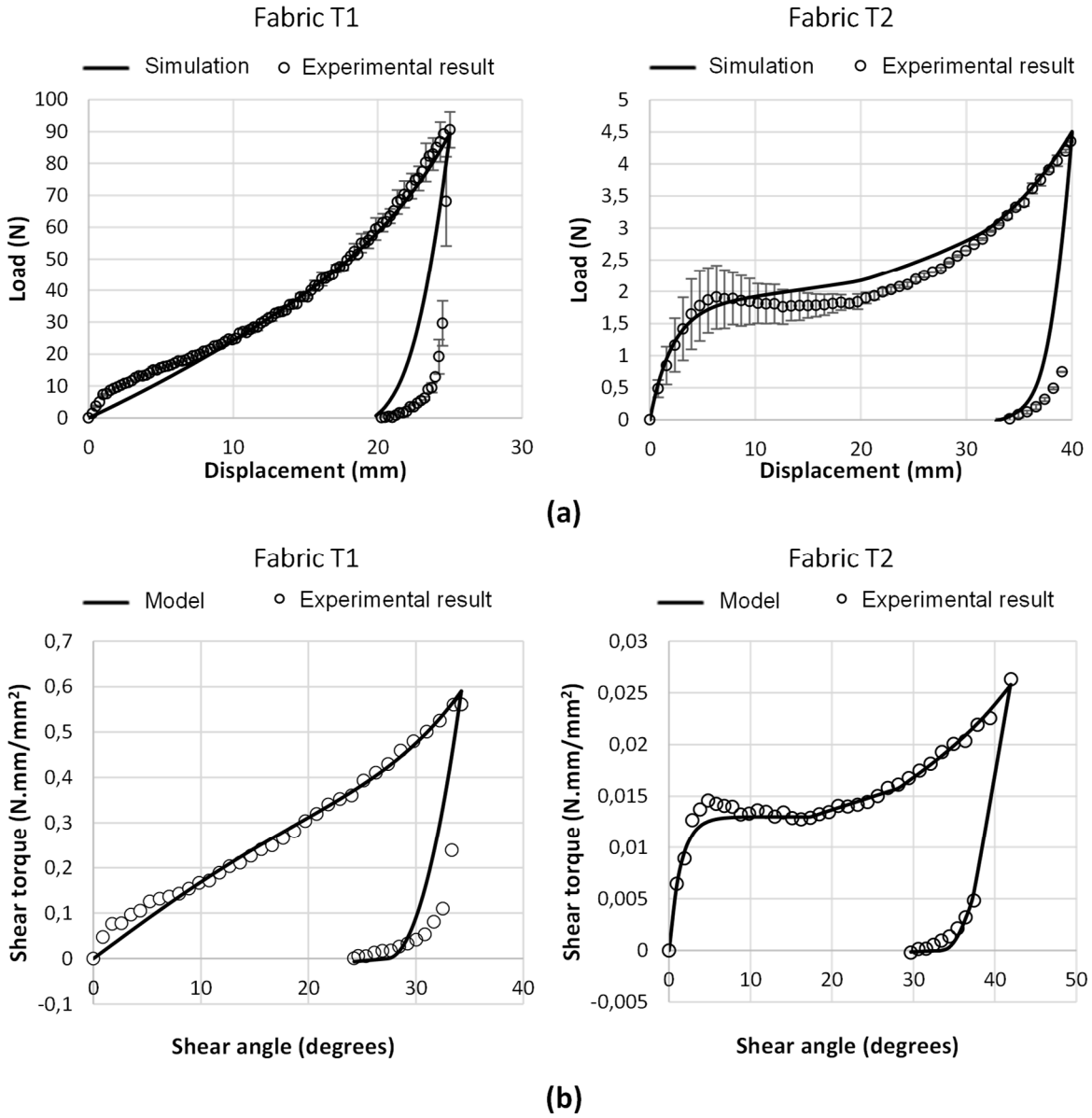

Fig. 5. Bias extension test: response to a loading/unloading. (a) Load versus displacement, (b) Shear torque versus shear angle.

2.3 Inelastic models

In order to be used in finite element simulations, simple models $M_b(\chi)$ and $C_s(\gamma)$ have been identified from the bending and in-plane shear tests.

The bending model gives the bending moment M_b as a function of the curvature χ. Two stages were considered: a loading stage for which the curvature increased, and an unloading stage for which the curvature decreased. The parameters of the following model was identified by best fit with the experimental data.

$$M_b(\chi) = \begin{cases} A\left(1 - e^{-\frac{\chi}{B}}\right) & \text{if } \frac{d\chi}{dt} \geq 0 \\ N \log\left(1 - \frac{\chi - \chi_r}{K}\right) & \text{if } \frac{d\chi}{dt} < 0 \end{cases} \quad (2)$$

Here, A, B, N and K are material parameters determined by the least square approach with the experimental results of Fig. 3b, and χ_r is the residual curvature (curvature corresponding to a zero bending moment during the unloading stage). All coefficients were determined in order to ensure that the $M_b(\chi)$ function be C^0 continuous. In the following, χ_{max} refers to the maximum curvature at the end of the loading stage. The parameters χ_r, K and N, which give the form of the relationship $M_b(\chi)$ during the unloading stage depend on the curvature χ_{max} from which the unloading stage is triggered. Fig. 6 shows the evolution of the parameters χ_r, K and N as functions of χ_{max} for several unloading stages for the fabric T1. These parameters evolve in a near-linear pattern with the value of χ_{max}. Using these relationships makes it possible to determine the unloading path for any value of χ_{max}.

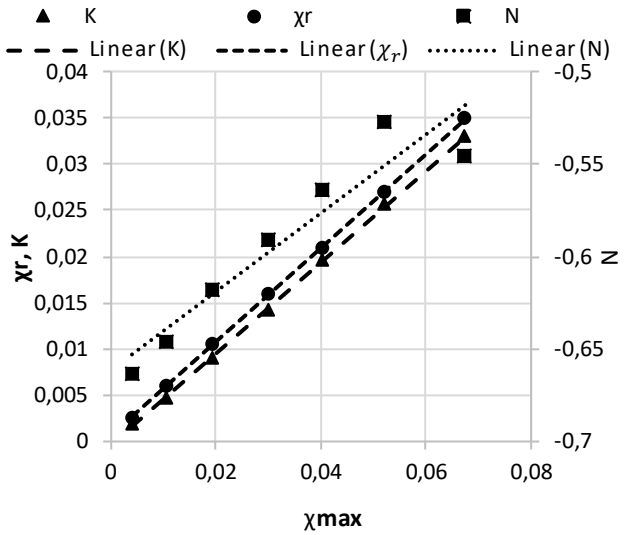

Fig. 6. Parameters χ_r, K and N of Eq. (2) vs the maximum curvature χ_{max}. The discontinuous lines represent the linear approximations.

The in-plane shear model gives the shear torque C_s as a function of the shear angle γ. The elastic part was assumed to be a fifth order polynomial function, as in previous works [26, 58]. The unloading part of the model was obtained by best fit with experimental data.

$$\begin{aligned} &\text{if } \frac{d\gamma}{dt} \geq 0 \quad C_s(\gamma) = K_1\gamma + K_3\gamma^3 + K_5\gamma^5 \\ &\text{if } \frac{d\gamma}{dt} < 0 \quad \text{if } \gamma \leq \gamma_r \quad C_s(\gamma) = b_0 + b_1\gamma \\ &\qquad\qquad\quad \text{if } \gamma > \gamma_r \; C_s(\gamma) = a_0 + a_1\gamma + a_2\gamma^2 \end{aligned} \tag{3}$$

Here, K_1, K_3 and K_5 are parameters describing the form of the loading stage (they are determined by curve fitting with the experimental results). γ_r is the residual shear angle (corresponding to zero shear torque in the unloading stage) and a_0, a_1, a_2, b_0 and b_1 are parameters that describe the unloading stage (they depend on the shear angle γ_{max} and shear torque $C_{s_{max}}$ at the end of the loading stage).

Fig. 3b and Fig. 5b show the identified models $M_b(\chi)$ and $C_s(\gamma)$ and compare them to the experimental curves. Fig. 3a displays the comparison between the load applied during bending in the middle of the specimen and that obtained by a finite element simulation using the model $M_b(\chi)$ (Eq. (2)) identified for the T1 and T2 reinforcements. Fig. 5a illustrates a comparison between the load on the bias extension test grips and that obtained by a finite element simulation using the $C_s(\gamma)$ model identified for the T1 and T2 reinforcements.

The models and experiments were in good agreement in all these cases. This was also true for the test presented in Fig. 4 consisting of several loadings and unloadings with increasing displacement. The models $M_b(\chi)$ and $C_s(\gamma)$ presented above were used in a draping simulation to investigate the importance of irreversibilities.

Two textile reinforcements were considered in the present study of the bending and in-plane shear behaviour. Although these reinforcements are quite different, the mechanical behaviour and irreversibilities are of the same nature and can be described by the same simple models. For the forming simulations below, only one woven fabric (T2=Hexcel G1151) was used in order to limit the number of results. The moment-curvature behaviour in the warp and weft directions are considered identical because the reinforcements are quasi-balanced.

3 Stress resultant shell element for textile reinforcements

The objective of textile reinforcement forming simulations is to determine the conditions necessary for the feasibility of the process, to gain knowledge of the position of the fibers after forming and to determine any defects, in particular wrinkles. Kinematic approaches (Fishnet) assume inextensible yarns and free rotation of yarns at cross over [7,8,59,60]. These methods are fast, but they do not take into account the mechanical behavior of the materials and the loads applied to the blank. An alternative lies in methods based on the equations of the mechanics which generally use a finite element approach [1,58,61-64]. Two review papers of the approaches used for the simulation of textile composite reinforcements have recently been published [4,29].

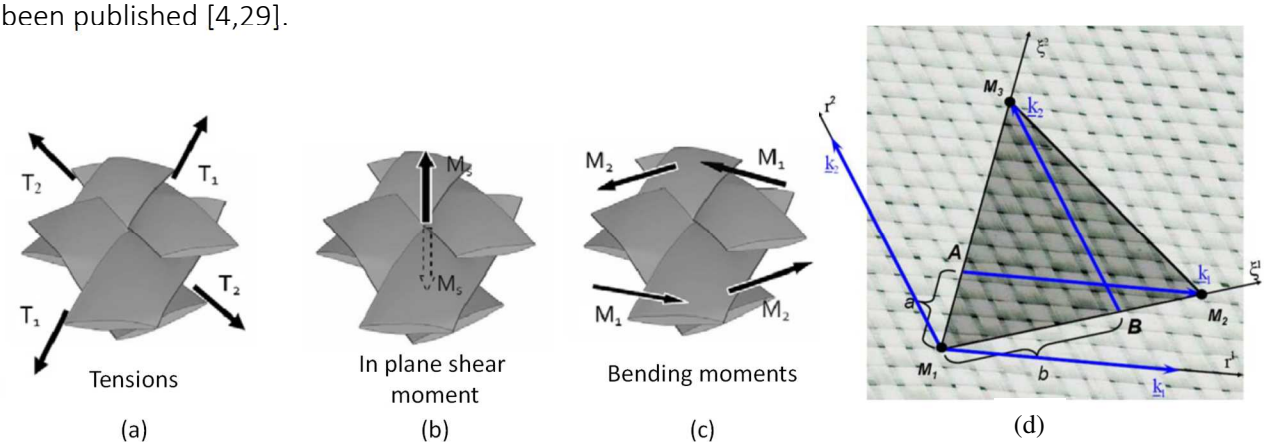

Fig. 7. Stress resultants on a woven unit cell: (a) tensions, (b) in-plane shear moment, (c) bending moments and (d) three node finite element made of woven cells.

The present work is based on stress resultants [58], an approach that distinguishes between the strain energies of tension, shear and bending and that is well suited for analyzing the influence of irreversibility during bending and shear.

It is assumed that the virtual work of the internal loads is the sum of those of tension (Fig. 7a and Eq. 4), in-plane shear (Fig. 7b and Eq. 4) and bending (Fig. 7c and Eq. 4). For a textile reinforcement composed of N_c woven cells, where the external virtual work is denoted $W_{ext}\left(\underline{\eta}\right)$ and the virtual work of acceleration quantities is expressed as $W_{acc}\left(\underline{\eta}\right)$, the principle of virtual work can be written:

$$W_{ext}\left(\underline{\eta}\right) - W_{acc}\left(\underline{\eta}\right) =$$

$$\sum_{p=1}^{N_c} {}^{p}\underbrace{\varepsilon_{11}\left(\underline{\eta}\right)\,{}^{p}T_1\,{}^{p}L_1 + {}^{p}\varepsilon_{22}\left(\underline{\eta}\right)\,{}^{p}T_2\,{}^{p}L_2}_{(a)} + \underbrace{\gamma\left(\underline{\eta}\right)\,{}^{p}C_s}_{(b)} + \underbrace{{}^{p}\chi_{11}\left(\underline{\eta}\right)\,{}^{p}M_{b_1}\,{}^{p}L_1 + {}^{p}\chi_{22}\left(\underline{\eta}\right)\,{}^{p}M_{b_2}\,{}^{p}L_2}_{(c)}$$

(4)

for any virtual displacement $\underline{\eta}$ equal to zero on the frontier with prescribed displacements.

The warp and weft lengths of the unit cell are denoted L_1 and L_2, the quantity ${}^{p}A$ corresponds to A for the unit cell p. ε_{11} and ε_{22} are the strain in the warp and weft directions. γ is the in-plane shear angle and χ_{11} and χ_{22} are the warp and weft curvatures respectively.

The stress resultant are assumed to be uncoupled, i. e. to depend only on the deformation directly associated with them (tensions $T_1(\varepsilon_{11}), T_2(\varepsilon_{22})$, in-plane shear moment $C_s(\gamma)$, bending moments $M_{b1}(\chi_{11}), M_{b2}(\chi_{22})$. Consequently, the internal loads are decoupled. Some studies have focused on the coupling between the stress resultants. In particular, tensions can influence the in-plane shear stiffness [15,65,66] and bending stiffness can be modified by in-plane shear [67,68]. However, these couplings are complex and for a given textile reinforcement, the data are generally not sufficient enough to be taken into account in forming simulations.

In Eq. (4), the shear torque C_s and the bending moment M_b experimentally analyzed and modeled in section 2 appear explicitly. There are two bending moments M_{b_1} and M_{b_2} in the warp and weft directions for a general loading. The bending virtual work due to the twisting curvature has been neglected in the present investigation. Moreover, irreversibilities in tension were not taken into account. The tensile strain of the fibers of composite textile reinforcements were small during the draping and it was assumed that the yarns remained elastic.

This simplified form of the principle of virtual work was used in a three-node triangular shell finite element with linear interpolation comprised of n_{celle} woven cells. The virtual works of the internal loads (Eq. (4)) gave the elementary internal nodal loads of tension $\mathbf{F}_{int}^{te}$, in-plane shear $\mathbf{F}_{int}^{se}$ and bending $\mathbf{F}_{int}^{be}$ as:

(a Eq. 4) (b Eq. 4) (c Eq. 4)

$$W_{int}^{te}\left(\underline{\eta}\right) = \boldsymbol{\eta}^{eT}\mathbf{F}_{int}^{te} \qquad W_{int}^{se}\left(\underline{\eta}\right) = \boldsymbol{\eta}^{eT}\mathbf{F}_{int}^{se} \qquad W_{int}^{be}\left(\underline{\eta}\right) = \boldsymbol{\eta}^{eT}\mathbf{F}_{int}^{be} \tag{5}$$

$$(\mathbf{F}_{int}^{te})_{ij} = n_{celle}\left(B_{1ij}T_1\frac{L_1}{||\underline{k}_1||^2} + B_{2ij}T_2\frac{L_2}{||\underline{k}_2||^2}\right) \tag{6}$$

$$(\mathbf{F}_{int}^{se})_{ij} = n_{celle}B_{\gamma ij}C_s \tag{7}$$

$$(\mathbf{F}_{int}^{be})_{km} = n_{celle}\left(Bb_{1km}M_{b_1}\frac{L_1}{||\underline{k}_1||^2} + Bb_{2km}M_{b_2}\frac{L_2}{||\underline{k}_2||^2}\right) \tag{8}$$

The internal nodal loads of bending stiffness are calculated within a rotation free approach [69,70]. In this technique, the locations of the neighbouring elements nodes are used to determine the curvatures. Here B_{1ij}, B_{2ij}, $B_{\gamma ij}$, Bb_{1km}, Bb_{2km} are strain interpolation components that are constant over the element because of the linear interpolation functions. $\underline{k}_1$ and $\underline{k}_2$ are the material vectors in the direction of the warp and weft yarns (Fig. 7d [62]):

$$\underline{k}_1 = \frac{\partial \underline{x}}{\partial r^1} \qquad \underline{k}_2 = \frac{\partial \underline{x}}{\partial r^2} \tag{9}$$

and r^1 and r^2 are material coordinates along the warp and weft yarns. The details of the calculations of these strain interpolations can be found in [58].

Eqs. (7) and (8) directly show the stress resultants C_s (in-plane shear moment), as well as M_{b_1} and M_{b_2} (bending moments) which were analyzed and modelled in section **2**. The models defined in Eqs. (2) and (3) were used in the following section, to take into account inelastic behaviors in bending and/or plane shear and to analyze the importance of the irreversibilities in forming simulations.

4 Forming simulations with elastic and inelastic behaviors

4.1 U-shape forming

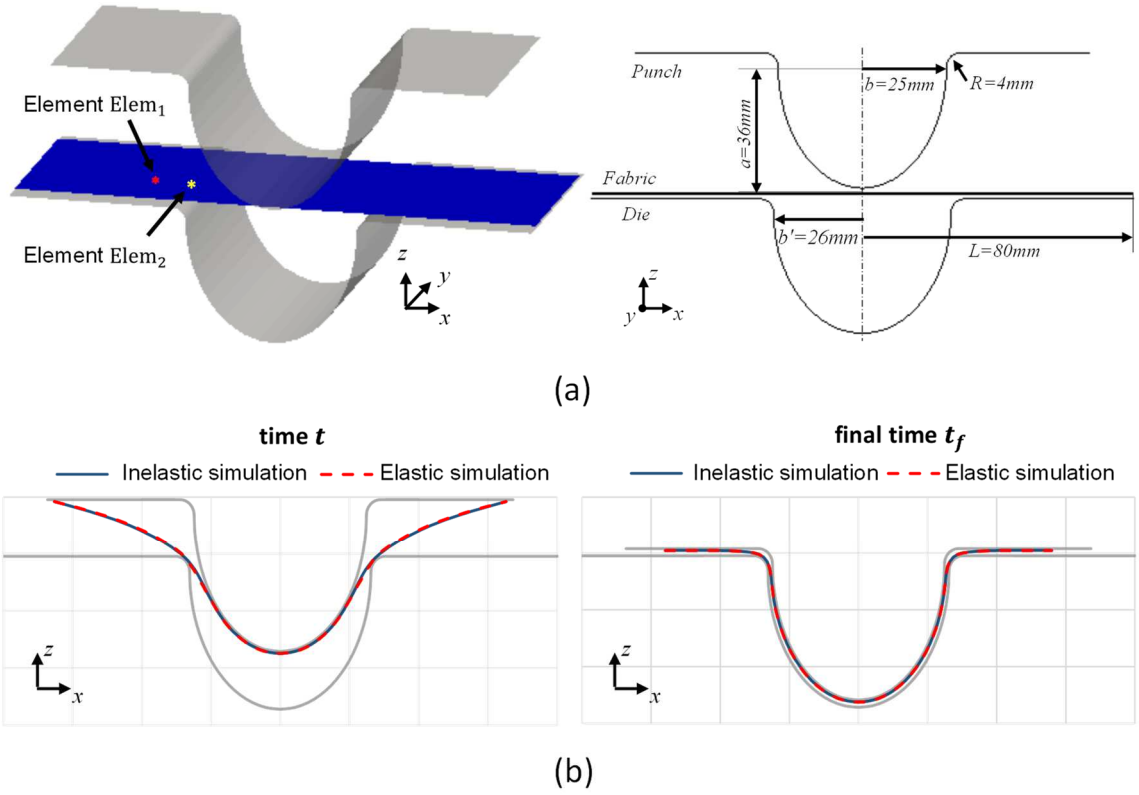

Fig. 8. U-shape forming, (a) geometry of tools, (b) reinforcement geometry during the forming (time $\boldsymbol{t}$) and at the end of the punch movement (time $\boldsymbol{t_f}$).

The first test was the forming of a U-shape as shown in Fig. 8a. This shape has a single curvature and the reinforcement T2 was considered. The initial form of the textile reinforcement was a 160 mm × 50 mm rectangle oriented at 0° and 90° with respect to the direction of the x-axis (50 woven cells). The fabric mesh comprised 6996 triangular elements. The contact and friction between the textile reinforcement and the tools is modelled by a Coulomb's law. The forward increment Lagrange multiplier method is used [71].

The evolution of the curvature during forming for elastic and inelastic simulations of two elements Elem_1 and Elem_2 is shown in Fig. 9a. The position of these two elements is presented in Fig. 8a. They underwent a curvature related to the die radius and then an inverse curvature related to the shape of the die, i.e., loading/unloading in bending. In general terms, the zones of the reinforcement that pass through the edge radii (the transition between the flat surface and the form cavity) were exposed to a non-monotonous bending moment and thus activated the inelastic mechanism.

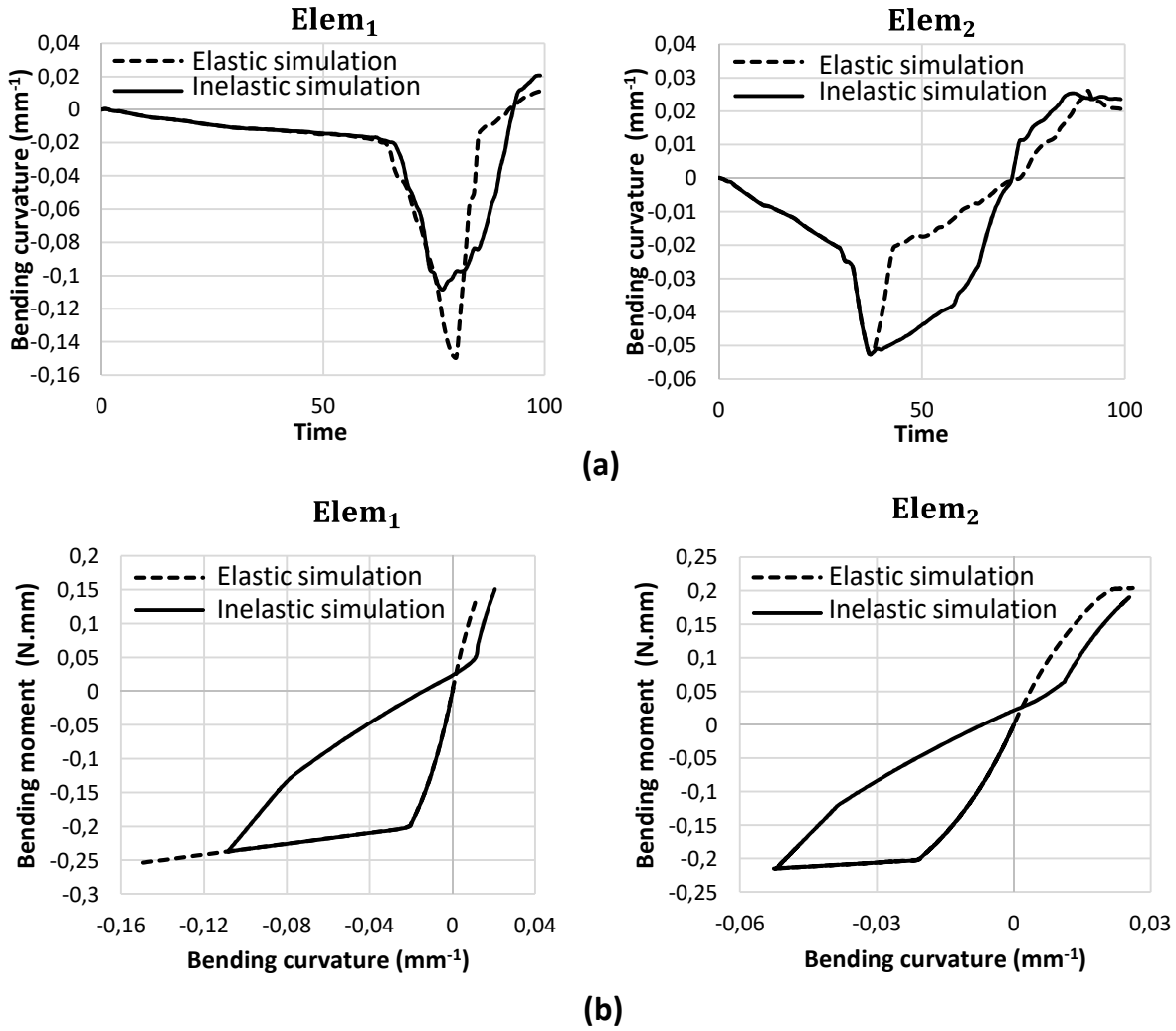

Fig. 9. (a) Bending curvature versus time (b) Bending moment versus bending curvature for element Elem1 and Elem2

Fig. 8b shows the deformed geometries of the textile reinforcement in the xz plane, corresponding to elastic and inelastic simulations at a time t related to a punch displacement of 24 mm as well as at the end of the simulation (the time t_f corresponds to a punch displacement of 40 mm). The difference in deflections obtained with these two simulations did not exceed 0.2 mm. Thus, with regard to the deformed geometry there was no significant difference between simulations based on an elastic vs an inelastic behavior model. This seemed reasonable given that the kinematics of the textile reinforcement were mainly imposed by the punch thus creating a monotonous path. The final shape was obtained if the punch met the die.

When it comes to bending moments, Fig. 9b displays that the ones calculated with the elastic and inelastic models differed in the second part of the forming process (after passing over the die radius). They were nevertheless rather close at the end of the punch movement.

The computed deformed geometry of the textile reinforcement at the end of the forming process was not significantly modified when taking into account irreversibilities in the mechanical behavior model. On the other hand, this geometry became significantly modified if the punch was removed. Fig. 10 portrays the reinforcement geometries, obtained by elastic and inelastic simulations, after the removal of the punch. These were very different. It is necessary to take the inelastic behavior into account in order to predict the deformed shape after the removal of the punch.

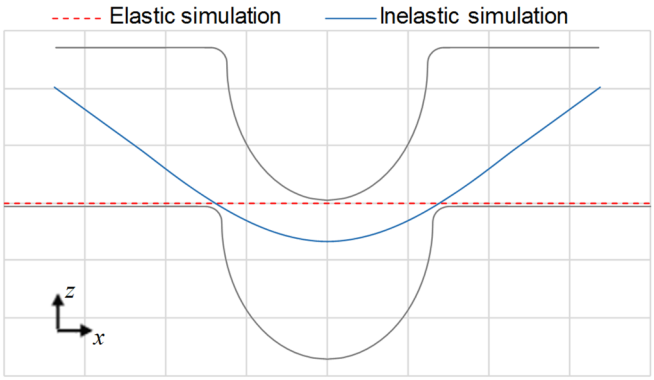

Fig. 10. Textile reinforcement shape after removing the punch

In a liquid infusion process, the punch is not removed and the mould remains closed. Nevertheless the simulation of the deformed shape after removing the punch shows that the behaviour of a textile reinforcement during forming is inherently irreversible and that it should in the general case be described by an inelastic model. In the case of preforming of LCM processes, elastic simulations can be considered given the monotonous nature of the process (the punch is not removed and the mould remains closed).

4.2 Hemispherical forming

The U-shape presented above is a single curved surface, that reduces the risk of wrinkles. This section presents a simulation of a hemispherical forming with elastic and inelastic behaviors. The hemisphere is a doubly-curved surface and the forming required shear angles which could lead to wrinkles. Forming was carried out without a blank holder.

The initial dimensions of the blank were 450 mm × 450 mm. Fig. 11a shows the geometry of the tools used in this forming process. The textile reinforcement T2 was considered. The yarns were initially at 0° (warp direction) and 90° (weft direction).

In this test, the points of the blank which pass through the radius of the die were subjected to loading and unloading in bending. There was no loading/unloading for the in-plane shear.

Fig. 11c shows the deformed geometries computed with elastic and inelastic models and they were found to be very close and in good agreement with the forming experiment (Fig. 11b). The vertical displacement difference was less than 2 mm for a blank size of 450 mm. Fig. 12 shows the norm for bending nodal forces (as defined in Eq. (7)). The differences between elastic and inelastic simulations were significant in the area around the die radius and in the wrinkles and these differences reached 40% in critical areas.

It is important to accurately calculate the internal moments at the end of the forming since they determine the internal stresses in the composite in case of LCM processes when a resin is injected in the textile preform after forming.

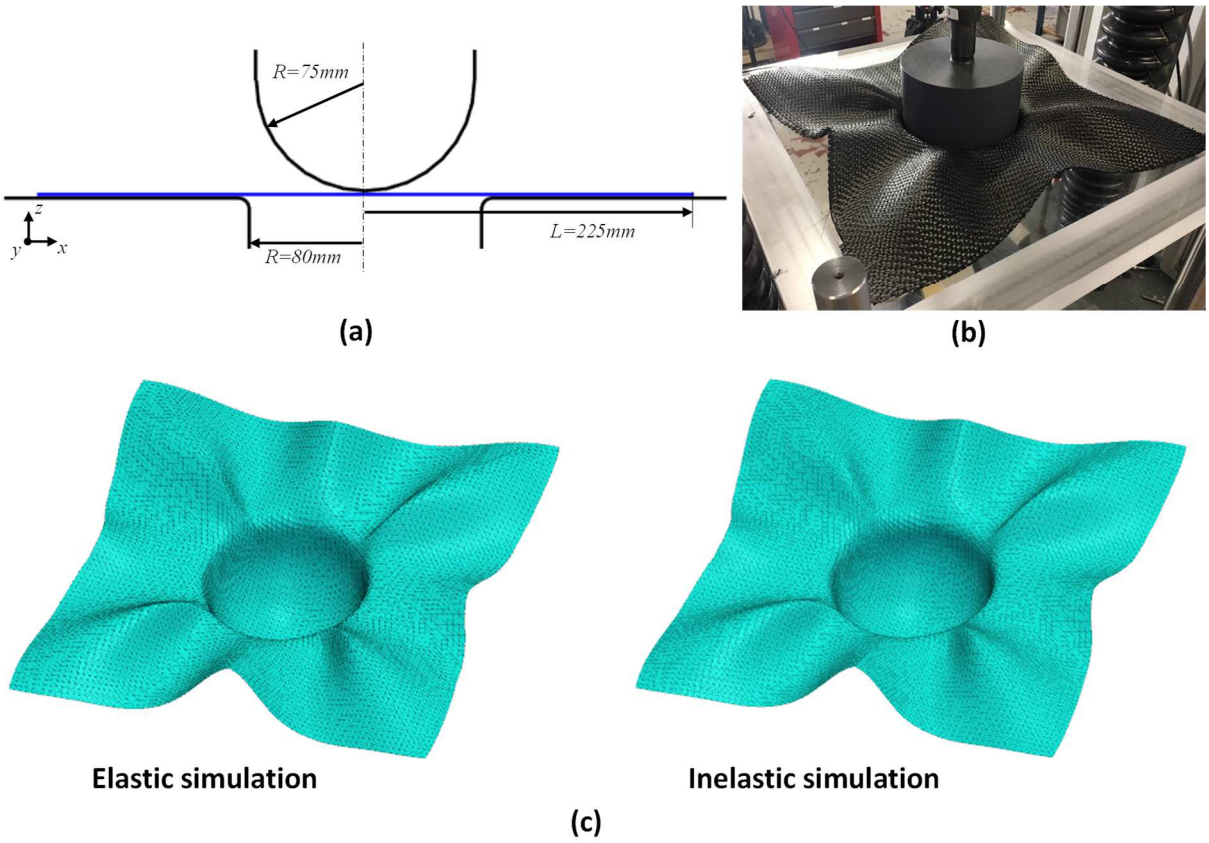

Fig. 11. Hemispherical forming. (a) Geometry of tools (2D view), (b) Experimental shape (c) and numerical shapes of the reinforcement at the end of the elastic and inelastic simulations.

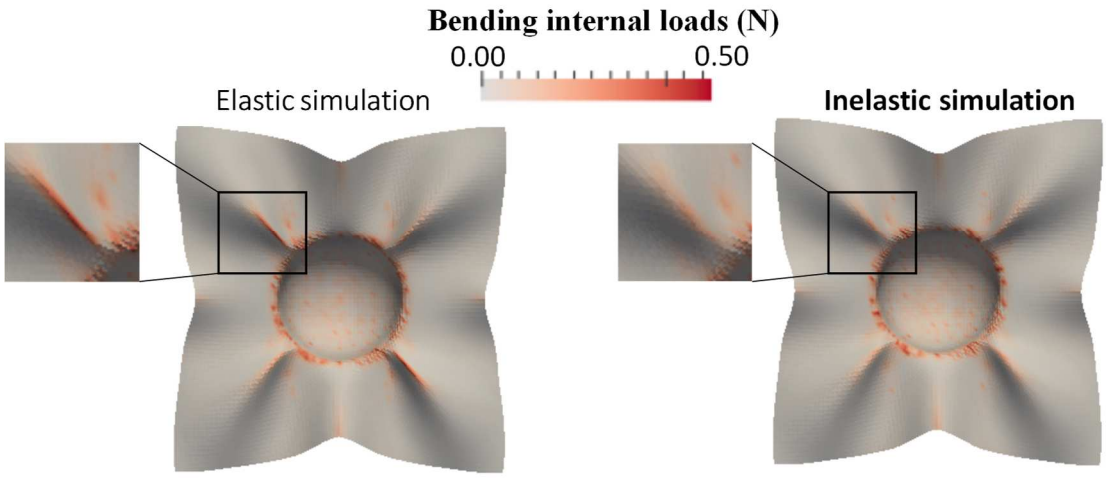

Fig. 12. Bending internal loads

4.3 Forming of a tetrahedral shape

The tetrahedron punch displayed in Fig. 13a and b has been used in several studies as a benchmark for strongly double curved forming [26,44,72-75]. The T2 textile reinforcement was initially a 700 mm × 700 mm square (3062 woven cell). The yarns were oriented at at 0° and 90° in the initial configuration. Fig. 13a and 13b shows the geometry of the tools. Six blank holders were used to avoid wrinkles in the tetrahedral part. This punch shape generated certain zones that underwent non-monotonous loads in bending as well as a few in in-plane shear. The inelastic behavior in bending and in-plane shear was taken into account in the simulation. The fabric mesh consisted of 40 000 triangular shell elements.

The final deformed shapes obtained by simulations using elastic and inelastic behavior showed small differences, essentially for wrinkles, for instance in zone A (Fig. 14). Both simulations are in fairly good agreement with the experiments (Fig. 13c) [26]. In particular, there weren't any wrinkles in either the experiment or the simulations in the tetrahedral part of the reinforcement. Fig. 13d confirms that some points underwent loading/unloading during in-plane shear (the element Elem_1 is located in zone A - Fig. 14). Nevertheless, these unloadings were very localized and had no tangible consequences on the final geometry. The difference in geometries obtained by the elastic and inelastic approaches remained smaller than 2 mm.

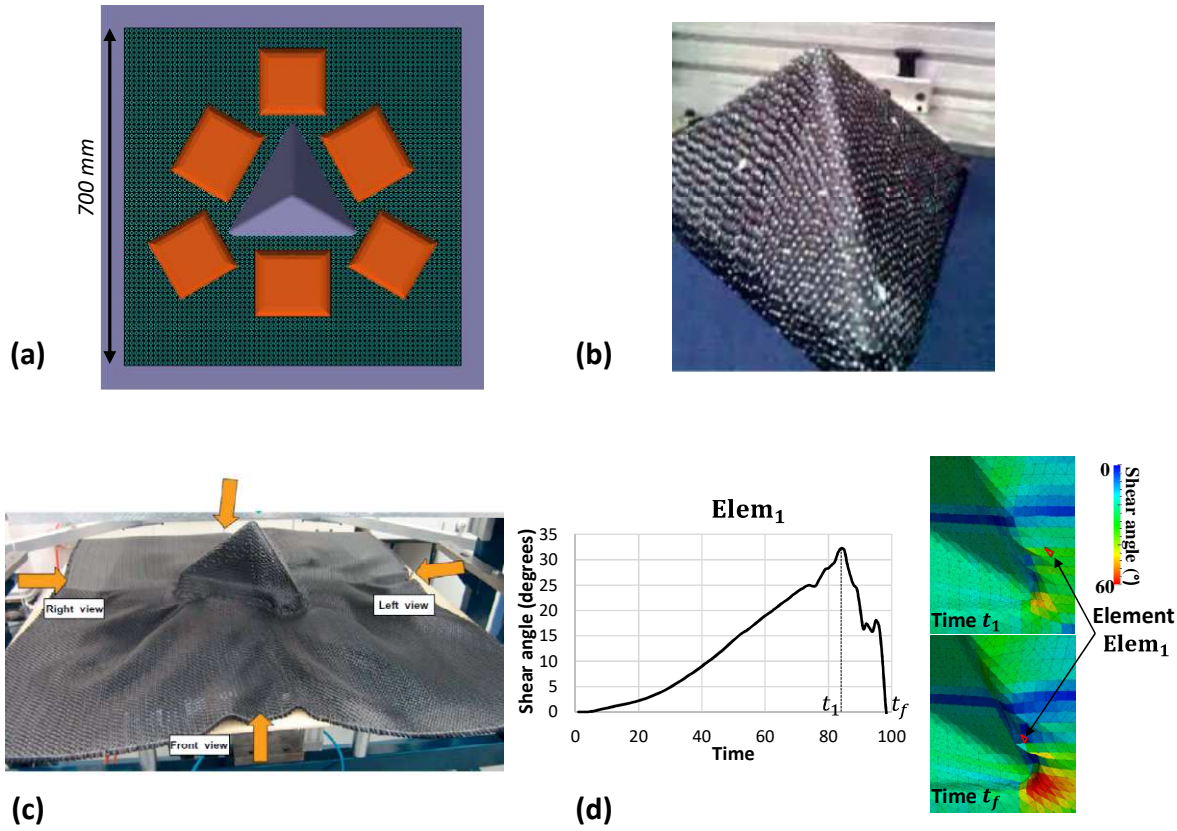

Fig. 13. Tetrahedral forming, (a and b) geometry of the tools, (c) forming experiment, (d) shear angle for element $\mathbf{Elem_1}$ during the forming.

The nodal bending and in-plane shear loads are presented in Fig. 14 for the elastic and inelastic simulations. The nodal bending loads were concentrated in the vicinity of the die radii and wrinkles. These were the areas where the curvature was at is maximum. The nodal shear loads were concentrated to the corners of the tetrahedron which corresponded to the points where the shear angles were at their highest. Differences were found between the values of these internal nodal loads when obtained with an elastic and inelastic approach. These differences reached up to 25% for nodal bending loads and 15% for nodal in-plane shear loads in critical areas.

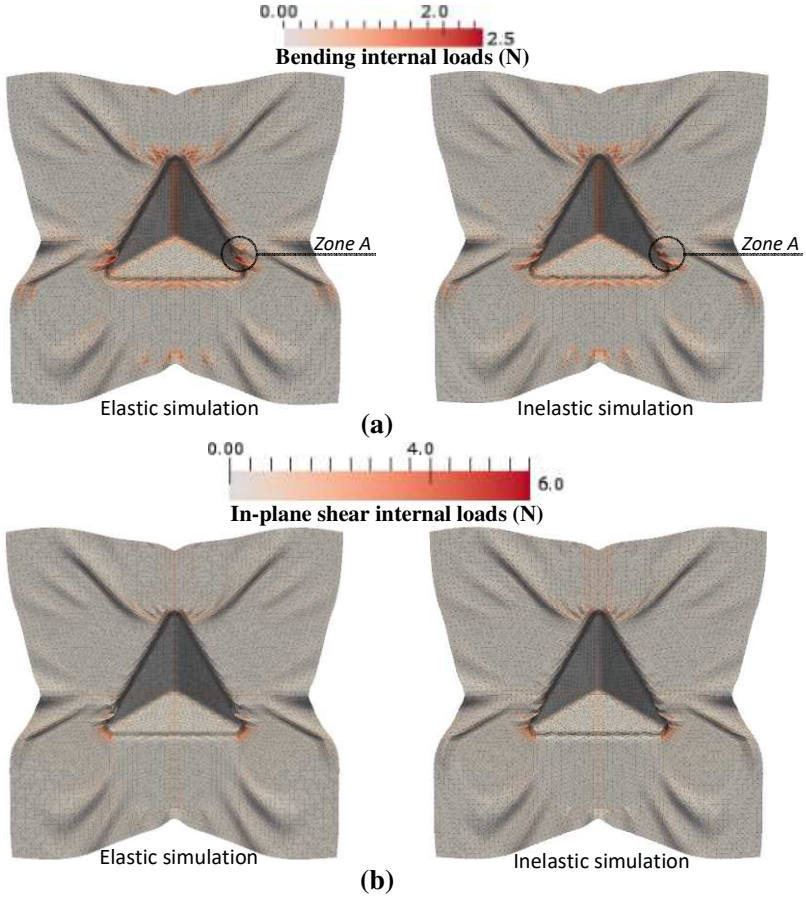

Fig. 14. (a) Bending internal loads, (b) in-plane shear internal loads.

Even though the difference between the shapes of the textile reinforcement obtained at the end of the punch displacement by elastic and inelastic simulations was small, it increased significantly if the punch was removed. In this case, the elastic simulation did not predict residual deformations and the textile reinforcement returned to its initial flat shape. Fig. 15 presents the shape of the reinforcement, obtained by an inelastic simulation, after removal of the punch. In case of a punch removal, the shapes obtained using an elastic vs. an inelastic model were definitely different.

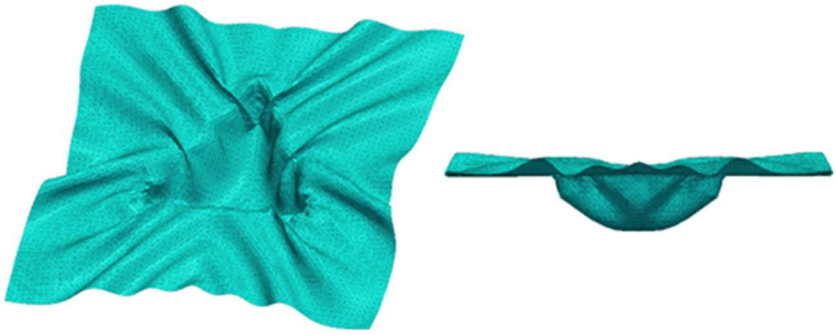

Fig. 15. Textile reinforcement shape after removal of the tetrahedral punch.

4.4 Box-shape forming

The geometry of the shape shown in Fig. 16a was made up of three rectangular boxes. This shape was one of the tests analyzed in the FiberMap European project [76,77]. Because of the three rectangular boxes, the shape had the particularity of creating in-plane shear loading/unloading for certain points of the textile reinforcement. The textile reinforcement T2 was considered with an orientation of 0°-90°.

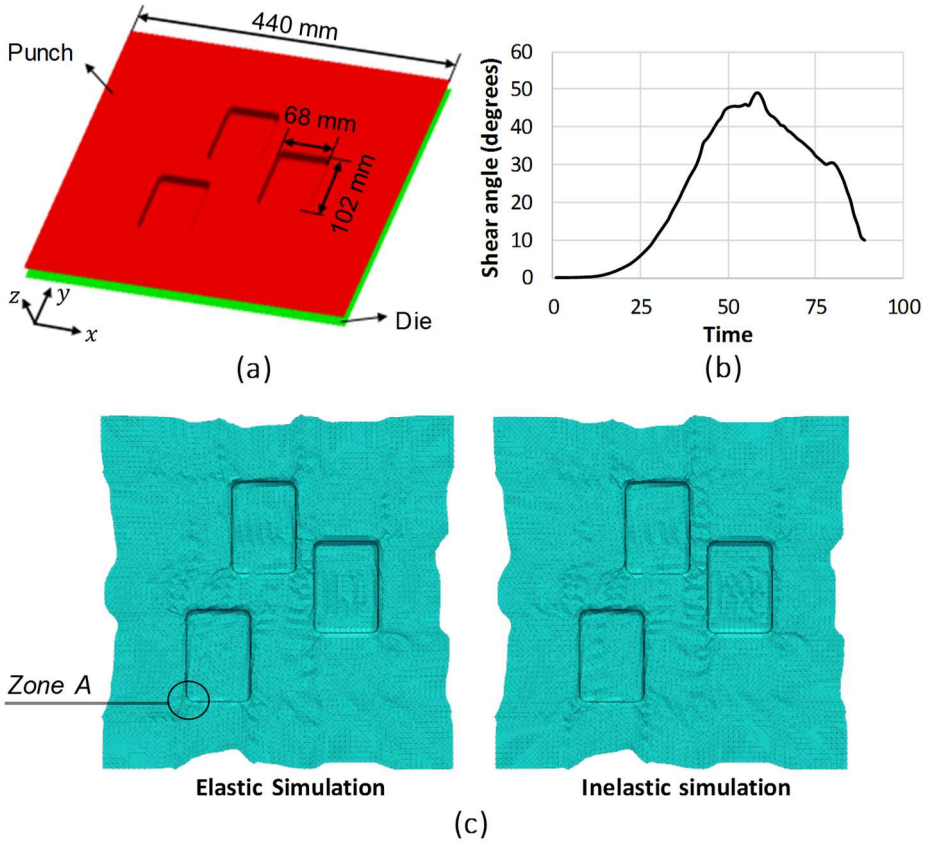

Fig. 16. Box-shape forming, (a) Tool geometry (b), shear angle (obtained by simulation) as a function of time for a point passing through zone A, and (c) deformed fabric geometry at the end of the simulation.

For textile reinforcement points passing through zone A (Fig. 16c), the shear angle increased. Due to the forming of the adjacent boxes, this point then moved into the flat bottom of the box causing the in-plane shear to decrease (Fig. 16b).

There was no significant difference concerning the final deformed geometry of textile reinforcement between elastic and inelastic simulations (Fig. 16c).

Regarding this type of forming, some zones of the fabric were exposed to loading/unloading in bending and others zones in in-plane shear. There were differences between the values of internal nodal loads in bending and in-plane shear obtained with an elastic and inelastic

approach (Fig. 17). These differences could reach up to 50% for nodal bending loads and 30% for nodal in-plane shear loads in critical areas.

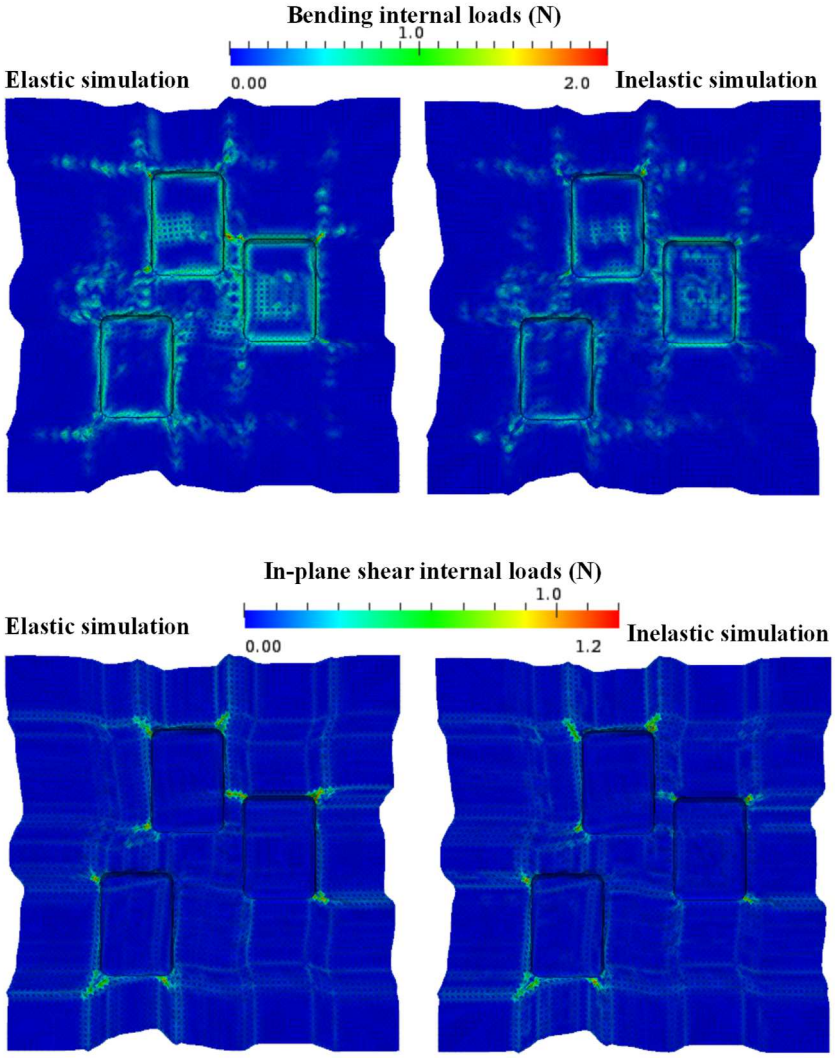

Fig. 17. Bending and in-plane shear internal loads for elastic and inelastic simulations.

When the resin is injected onto a preform, the internal forces obtained at the end of preforming are not relaxed and constitute a source of internal stresses in the composite in service (with hardened resin). An analysis of the consequences of internal stresses in the composite in service would therefore require the consideration of irreversibilities in the prior simulation of the preforming in order to obtain relevant internal forces.

5 Conclusion

Irreversibilities in the mechanical behavior of textile composite reinforcements during forming have been considered in bending and in-plane shear tests. These irreversibilities

were caused by the slippage between the fibers and the associated friction that occured during forming. They were clearly shown by bending and shear tests. Taking these irreversibilities into account in the forming simulations made it possible to compare the solutions then obtained with the elastic simulations. When the forming was carried out by a monotonous displacement of the punch (the most frequent case), the computed deformed geometry of the reinforcement was not significantly modified by taking into account irreversibilities in the mechanical behavior model. This was very different when considering the removal of the punch (see sections 4.1 and 4.3 for U-shape and tetrahedron forming). In this case, the geometry after removal of the punch could only be correctly obtained by taking into account the inelastic aspects of the behavior.

During a monotonous displacement of the punch, the parts of the reinforcements that passed over the radii of the die underwent loading/unloading of the curvatures and bending moments. As a result, the internal loads were modified by taking into account irreversibilities in the simulation. In conclusion, simulations based on elastic models generally sufficied to determine deformations in forming processes with monotonous tool displacement. The analysis of internal loads in textile reinforcement was more relevant when the irreversibilities of behavior were taken into account. They can be significant with regard to internal stresses in the composite in case of LCM processes. The results presented here concern dry textile reinforcements. In the case of thermosetting or thermoplastic prepregs, the resin provides a viscous contribution that also has to be modeled.

The employed model was empirical and non-unique since it was based on a best fit to structural tests. Hence, the conclusions of this paper are only valid for the characterization and modeling strategy used. These conclusions may indeed be true in general, but to demonstrate them effectively would require additional analyses on a set of materials and with enhanced models.

Experimental shaping was presented in the case of forming with a hemispherical and tetrahedral punch and used to validate the simulations. The extension of these experimental analyses to U-shape and box-shape forming cases and especially to punch removal cases should make it possible to validate the modeling strategy.

Acknowledgements

This work was supported by the French Ministry of Higher Education and Research

References

[1] De Luca P, Lefébure P, Pickett AK. Numerical and experimental investigation of some press forming parameters of two fibre reinforced thermoplastics: APC2-AS4 and PEI-CETEX. Composites Part A: Applied Science and Manufacturing 1998;29(1-2):101-110.

[2] Boisse P, Hamila N, Vidal-Sallé E, Dumont F. Simulation of wrinkling during textile composite reinforcement forming. Influence of tensile, in-plane shear and bending stiffnesses. Composites Science and Technology 2011;71(5):683-692.

[3] Walther J, Simacek P, Advani SG. The effect of fabric and fiber tow shear on dual scale flow and fiber bundle saturation during liquid molding of textile composites. International journal of material forming 2012;5(1):83-97.

[4] Gereke T, Döbrich O, Hübner M, Cherif C. Experimental and computational composite textile reinforcement forming: a review. Composites Part A: Applied Science and Manufacturing 2013;46:1-10.

[5] Dangora LM, Mitchell CJ, Sherwood JA. Predictive model for the detection of out-of-plane defects formed during textile-composite manufacture. Composites Part A: Applied Science and Manufacturing 2015;78:102-112.

[6] Mallach A, Härtel F, Heieck F, Fuhr JP, Middendorf P, Gude M. Experimental comparison of a macroscopic draping simulation for dry non-crimp fabric preforming on a complex geometry by means of optical measurement. Journal of Composite Materials 2017;51(16):2363-2375.

[7] Long AC, Rudd CD. A simulation of reinforcement deformation during the production of preforms for liquid moulding processes. Proceedings of the Institution of Mechanical Engineers, Part B: Journal of Engineering Manufacture 1994;208(4):269-278.

[8] Potter K. Beyond the pin-jointed net: maximising the deformability of aligned continuous fibre reinforcements. Composites Part A: Applied Science and Manufacturing 2002;33(5):677-686.

[9] Cherouat A, Borouchaki H, Giraud-Moreau L. Mechanical and geometrical approaches applied to composite fabric forming. International journal of material forming 2010;3(2):1189-1204.

[10] Ten Thije RHW, Akkerman R. A multi-layer triangular membrane finite element for the forming simulation of laminated composites. Composites Part A: Applied Science and Manufacturing 2009;40(6-7):739-753.

[11] Durville D. Simulation of the mechanical behaviour of woven fabrics at the scale of fibers. International journal of material forming 2010;3(2):1241-1251.

[12] Lin H, Wang J, Long AC, Clifford MJ, Harrison P. Predictive modelling for optimization of textile composite forming. Composites Science and Technology 2007;67(15-16):3242-3252.

[13] Lee JS, Hong SJ, Yu WR, Kang TJ. The effect of blank holder force on the stamp forming behavior of non-crimp fabric with a chain stitch. Composites science and technology 2007;67(3-4):357-366.

[14] Skordos AA, Aceves CM, Sutcliffe MP. A simplified rate dependent model of forming and wrinkling of pre-impregnated woven composites. Composites Part A: Applied science and manufacturing 2007;38(5):1318-1330.

[15] Harrison P, Abdiwi F, Guo Z, Potluri P, Yu WR. Characterising the shear–tension coupling and wrinkling behaviour of woven engineering fabrics. Composites Part A: Applied science and manufacturing 2012;43(6):903-914.

[16] Rudd CD, Long AC. Liquid Molding Technologies, Cambridge: Woodhead Pub, 1997.

[17] Advani SG, Hsiao KT. (Eds.). Manufacturing techniques for polymer matrix composites (PMCs). Elsevier, 2012.

[18] Bickerton, S., Šimácek, P., Guglielmi, S. E., & Advani, S. G. Investigation of draping and its effects on the mold filling process during manufacturing of a compound curved composite part. Composites Part A: Applied Science and Manufacturing 1997;28(9-10):801-816.

[19] Wang, P., Drapier, S., Molimard, J., Vautrin, A., & Minni, J. C. Characterization of Liquid Resin Infusion (LRI) filling by fringe pattern projection and in situ thermocouples. Composites Part A: Applied Science and Manufacturing 2010;41(1):36-44.

[20] Park, C. H., Lebel, A., Saouab, A., Bréard, J., & Lee, W. I. Modeling and simulation of voids and saturation in liquid composite molding processes. Composites Part A: Applied science and manufacturing 2011:42(6):658-668.

[21] Caglar, B., Orgéas, L., Du Roscoat, S. R., Sozer, E. M., & Michaud, V. Permeability of textile fabrics with spherical inclusions. Composites Part A: Applied Science and Manufacturing 2017; 99:1-14.

[22] Bancora, S. P., Binetruy, C., Advani, S. G., Syerko, E., & Comas-Cardona, S. Effective permeability averaging scheme to address in-plane anisotropy effects in multi-layered preforms. Composites Part A: Applied Science and Manufacturing 2018:113: 359-369.

[23] Rahali, Y., Assidi, M., Goda, I., Zghal, A., & Ganghoffer, J. F. (2016). Computation of the effective mechanical properties including nonclassical moduli of 2.5 D and 3D interlocks by micromechanical approaches. Composites Part B: Engineering, 98, 194-212.

[24] Peng XQ, Cao J. A continuum mechanics-based non-orthogonal constitutive model for woven composite fabrics. Composites part A: Applied Science and manufacturing 2005;36(6):859-874.

[25] Jauffrès D, Sherwood JA, Morris CD, Chen J. Discrete mesoscopic modeling for the simulation of woven-fabric reinforcement forming. International Journal of Material Forming 2010;3(2):1205-1216.

[26] Allaoui S, Boisse P, Chatel S, Hamila N, Hivet G, Soulat D, Vidal-Salle E. Experimental and numerical analyses of textile reinforcement forming of a tetrahedral shape. Composites Part A: Applied Science and Manufacturing 2011;42(6):612-622.

[27] Peng X, Rehman ZU. Textile composite double dome stamping simulation using a non-orthogonal constitutive model. Composites Science and Technology 2011;71(8):1075-1081.

[28] Schirmaier FJ, Dörr D, Henning F, Kärge L. A macroscopic approach to simulate the forming behaviour of stitched unidirectional non-crimp fabrics (UD-NCF). Composites Part A: Applied Science and Manufacturing 2017;102:322-335.

[29] Bussetta P, Correia N. Numerical forming of continuous fibre reinforced composite material: A review. Composites Part A: Applied Science and Manufacturing 2018;113:12-31.

[30] Yu W R, Harrison P, Long A. Finite element forming simulation for non-crimp fabrics using a non-orthogonal constitutive equation. Composites Part A: Applied Science and Manufacturing 2005;36(8):1079-1093.

[31] Boisse P, Hamila N, Helenon F, Hagège B, Cao J. Different approaches for woven composite reinforcement forming simulation. International Journal of Material Forming 2008;1(1):21-29.

[32] Khan MA, Mabrouki T, Vidal-Sallé E, Boisse P. Numerical and experimental analyses of woven composite reinforcement forming using a hypoelastic behaviour. Application to the double dome benchmark. Journal of materials processing technology 2010;210(2):378-388.

[33] Charmetant A, Orliac JG, Vidal-Sallé E, Boisse P. Hyperelastic model for large deformation analyses of 3D interlock composite preforms. Composites Science and Technology 2012;72(12):1352-1360.

[34] Gong Y, Peng X, Yao Y, Guo Z. An anisotropic hyperelastic constitutive model for thermoplastic woven composite prepregs. Composites Science and Technology 2016;128:17-24.

[35] Haanappel SP, Ten Thije RHW, Sachs U, Rietman B, Akkerman R. Formability analyses of uni-directional and textile reinforced thermoplastics. Composites Part A: Applied science and manufacturing 2014;56:80-92.

[36] Belnoue, J. H., Nixon-Pearson, O. J., Ivanov, D., & Hallett, S. R. A novel hyper-viscoelastic model for consolidation of toughened prepregs under processing conditions. Mechanics of Materials, 2016: 97: 118-134.

[37] Guzman-Maldonado E, Hamila N, Naouar N, Moulin G, Boisse P. Simulation of thermoplastic prepreg thermoforming based on a visco-hyperelastic model and a thermal homogenization. Materials & Design 2016;93:431-442.

[38] Dörr D, Schirmaier FJ, Henning F, Kärger L. A viscoelastic approach for modeling bending behavior in finite element forming simulation of continuously fiber reinforced composites. Composites Part A: Applied Science and Manufacturing 2017;94:113-123.

[39] Denis Y, Guzman-Maldonado E, Hamila N, Colmars J, Morestin F. A dissipative constitutive model for woven composite fabric under large strain. Composites Part A: Applied Science and Manufacturing 2018;105:165-179.

[40] Barlat F, Lian K. Plastic behavior and stretchability of sheet metals. Part I: A yield function for orthotropic sheets under plane stress conditions. International journal of plasticity 1989;5(1):51-66.

[41] Barlat F, Brem JC, Yoon JW, Chung K, Dick RE, Lege DJ, Pourboghrat F, Choi SH, Chu E. Plane stress yield function for aluminum alloy sheets—part 1: theory. International Journal of Plasticity 2003;19(9):1297-1319.

[42] Simo JC, Hughes TJ. Computational inelasticity (Vol. 7). Springer Science & Business Media, 2006.

[43] Naouar, N., Vidal-Salle, E., Schneider, J., Maire, E., Boisse, P.. 3D composite reinforcement meso FE analyses based on X-ray computed tomography. Composite Structures, 2015, 132, 1094-1104.

[44] Pazmino J, Carvelli V, Lomov SV. Formability of a non-crimp 3D orthogonal weave E-glass composite reinforcement. Composites Part A: Applied Science and Manufacturing 2014;61:76-83.

[45] Lomov SV, Boisse P, Deluycker E, Morestin F, Vanclooster K, Vandepitte D, Verpoest I, Willems A. Full-field strain measurements in textile deformability studies. Composites Part A: Applied Science and Manufacturing 2008;39(8):1232-1244.

[46] Launay J, Hivet G, Duong AV, Boisse P. Experimental analysis of the influence of tensions on in plane shear behaviour of woven composite reinforcements. Composites science and technology 2008;68(2):506-515.

[47] Peirce FT. 26—The “handle” of cloth as a measurable quantity. Journal of the Textile Institute Transactions 1930;21(9):T377-T416.

[48] Lomov SV, Truevtzev AV, Cassidy C. A predictive model for the fabric-to-yarn bending stiffness ratio of a plain-woven set fabric. Textile research journal 2000;70(12):1088-1096.

[49] Boisse P, Colmars J, Hamila N, Naouar N, Steer Q. Bending and wrinkling of composite fiber preforms and prepregs. A review and new developments in the draping simulations. Composites Part B: Engineering 2018;141:234-249.

[50] Mathieu, S., Hamila, N., Bouillon, F., & Boisse, P. Enhanced modeling of 3D composite preform deformations taking into account local fiber bending stiffness. Composites Science and Technology, 2015, 117, 322-333.

[51] Madeo, A., Ferretti, M., Dell’Isola, F., & Boisse, P. (2015). Thick fibrous composite reinforcements behave as special second-gradient materials: three-point bending of 3D interlocks. Zeitschrift für angewandte Mathematik und Physik, 66(4), 2041-2060.

[52] Lebrun G, Bureau MN, Denault J. Evaluation of bias-extension and picture-frame test methods for the measurement of intraply shear properties of PP/glass commingled fabrics. Composite structures 2003;61(4):341-352.

[53] Harrison P, Clifford MJ, Long AC. Shear characterisation of viscous woven textile composites: a comparison between picture frame and bias extension experiments. Composites science and technology 2004;64(10-11):1453-1465.

[54] Cao J, Akkerman R, Boisse P, Chen J, Cheng HS, De Graaf EF, ..., Lee W. Characterization of mechanical behavior of woven fabrics: experimental methods and benchmark results. Composites Part A: Applied Science and Manufacturing 2008;39(6):1037-1053.

[55] D'Agostino MV, Giorgio I, Greco L, Madeo A, Boisse P. Continuum and discrete models for structures including (quasi-) inextensible elasticae with a view to the design and modeling of composite reinforcements. International Journal of Solids and Structures 2015;59:1-17.

[56] Boisse P, Hamila N, Guzman-Maldonado E, Madeo A, Hivet G, Dell'Isola F. The bias-extension test for the analysis of in-plane shear properties of textile composite reinforcements and prepregs: a review. International Journal of Material Forming 2017;10(4):473-492.

[57] Liang, B., Chaudet, P., & Boisse, P. Curvature determination in the bending test of continuous fibre reinforcements. Strain 2017;53(1):e12213.

[58] Hamila N, Boisse P, Sabourin F, Brunet M. A semi-discrete shell finite element for textile composite reinforcement forming simulation. International journal for numerical methods in engineering 2009;79(12):1443-1466.

[59] Wang J, Page JR, Paton R. Experimental investigation of the draping properties of reinforcement fabrics. Composites Science and Technology 1998;58(2):229-237.

[60] Potluri P, Sharma S, Ramgulam R. Comprehensive drape modelling for moulding 3D textile preforms. Composites Part A: Applied science and manufacturing 2001;32(10):1415-1424.

[61] Pickett AK. Review of finite element simulation methods applied to manufacturing and failure prediction in composites structures. Applied Composite Materials 2002;9(1):43-58.

[62] Hamila, N., & Boisse, P. (2007). A meso–macro three node finite element for draping of textile composite preforms. Applied composite materials, 14(4), 235-250.

[63] Ten Thije RHW, Akkerman R, Huétink J. Large deformation simulation of anisotropic material using an updated Lagrangian finite element method. Computer methods in applied mechanics and engineering 2007;196(33-34):3141-3150.

[64] Peng X, Ding F. Validation of a non-orthogonal constitutive model for woven composite fabrics via hemispherical stamping simulation. Composites Part A: Applied Science and Manufacturing 2011;42(4):400-407.

[65] Yao, Y., Peng, X., & Gong, Y. (2019). Influence of tension–shear coupling on draping of plain weave fabrics. Journal of materials science, 54(8), 6310-6322.

[66] Yao, Y., Huang, X., Peng, X., Liu, P., & Youkun, G. (2019). An anisotropic hyperelastic constitutive model for plain weave fabric considering biaxial tension coupling. Textile Research Journal, 89(3), 434-444.

[67] Mitchell, C., Dangora, L., Bielmeier, C., & Sherwood, J. (2016). Investigation into the changes in bending stiffness of a textile reinforced composite due to in-plane fabric shear: Part 1–Experiment. Composites Part A: Applied Science and Manufacturing, 85, 94-102.

[68] Mitchell, C., Dangora, L., Bielmeier, C., & Sherwood, J. (2016). Investigation into the changes in bending stiffness of a textile reinforced composite due to in-plane fabric shear: Part 2–Numerical analysis. Composites Part A: Applied Science and Manufacturing, 85, 138-147.

[69] Onate E, Zárate F. Rotation-free triangular plate and shell elements. International Journal for Numerical Methods in Engineering 2000;47(1-3):557-603.

[70] Sabourin F, Brunet M. Detailed formulation of the rotation-free triangular element “S3” for general purpose shell analysis. Engineering computations 2006;23(5):469-502.

[71] Carpenter, N. J., Taylor, R. L., & Katona, M. G. (1991). Lagrange constraints for transient finite element surface contact. International journal for numerical methods in engineering, 32(1), 103-128.

[72] Ouagne P, Soulat D, Moothoo J, Capelle E, Gueret S. Complex shape forming of a flax woven fabric; analysis of the tow buckling and misalignment defect. Composites Part A: Applied Science and Manufacturing 2013;51:1-10.

[73] Allaoui S, Hivet G, Soulat D, Wendling A, Ouagne P, Chatel S. Experimental preforming of highly double curved shapes with a case corner using an interlock reinforcement. International Journal of Material Forming 2014;7(2):155-165.

[74] Pazmino J, Mathieu S, Carvelli V, Boisse P, Lomov SV. Numerical modelling of forming of a non-crimp 3D orthogonal weave E-glass composite reinforcement. Composites Part A: Applied Science and Manufacturing 2015;72:207-218.

[75] Thompson AJ, El Said B, Belnoue JP, Hallett SR. Modelling process induced deformations in 0/90 non-crimp fabrics at the meso-scale. Composites Science and Technology 2018;168:104-110.

[76] FibreMap, http://fibremap.eu/, Automatic Mapping of Fibre Orientation of Carbon Fibre Parts, Europeen project FP7 2014-2016.

[77] Colmars J, Rusanov A, Ta AT, Naouar N, Boisse P. Fibre mapping analysis in composite forming: Experimental and numerical comparison. In AIP Conference Proceedings. AIP Publishing, October, 2016. p. 170027.